Chinese Chemical Letters 36 (2025) 110286

Contents lists available at ScienceDirect

Chinese Chemical Letters

journal homepage: www.elsevier.com/locate/cclet

In situ preparation of tannin-mediated CeO_2@CuS nanocomposites for multimodal wound therapy

Hongwei Ding[a], Jingjing Yang[b], Yongchen Shuai[b], Di Wei[b], Xueliang Liu[a], Guiying Li[d,*], Lin Jin[a,*], Jianliang Shen[c,*]

[a] *The Key Laboratory of Rare Earth Functional Materials and Applications, International Joint Research Laboratory for Biomedical Nanomaterials of Henan, Zhoukou Normal University, Zhoukou 466001, China*
[b] *School of Chemistry and Chemical Engineering, Zhoukou Normal University, Zhoukou 466001, China*
[c] *Zhejiang Engineering Research Center for Tissue Repair Materials, Wenzhou Institute, University of Chinese Academy of Sciences, Wenzhou 325001, China*
[d] *Affiliated Hospital of Hebei Engineering University, The Key Laboratory of Basic Research on Blood Purification Application in Hebei Province, Handan 056002, China*

ARTICLE INFO

Article history:
Received 11 June 2024
Revised 16 July 2024
Accepted 18 July 2024
Available online 19 July 2024

Keywords:
Nanocomposites
Antibacterial
Anti-inflammation
Wound therapy
Photothermal
ROS scavenging

ABSTRACT

Bacterial infection, insufficient angiogenesis, and oxidative damage are generally regarded as key issues that impede wound healing, making it necessary to prepare new biomaterials to simultaneously address these problems. In this work, monodispersed CeO_2@CuS nanocomposites (NCs) were successfully prepared with tannin (TA) as the reductant and linker. Due to abundant oxygen vacancies in CeO_2 and the polyphenolic structure of TA, the TA-CeO_2@CuS NCs exhibited a remarkable antioxidant ability to scavenge excessive reactive oxygen species (ROS), which would likely induce serious inflammation. In addition, the TA-CeO_2@CuS NCs demonstrated excellent antibacterial capability with near-infrared ray (NIR) irradiation, and the released copper ions could promote the regeneration of blood vessels. These synergistic effects indicated that the synthesized TA-CeO_2@CuS NCs could serve as a promising biomaterial for multimodal wound therapy.

Wound management is a significant challenge worldwide, causing significant suffering among patients and an enormous financial burden on governments [1,2]. Numerous noteworthy treatments exist that can accelerate wound healing, such as antisepsis, anti-inflammation, and the promotion of angiogenesis [3-5]. However, the traditional drugs and dressings usually have single functionality and unsatisfactory effects, making it necessary to develop new types of biomaterials for multimodal synergetic wound therapy [6,7].

Excessive reactive oxygen species (ROS) and bacterial infections would lead to serious inflammatory response, hindering or even endangering wound healing [8-10]. Therefore, wound healing may be accelerated by effectively obtaining antioxidant species and maintaining the balance of redox in cells [11,12]. Due to abundant oxygen vacancies on the surfaces of cerium dioxide nanoparticles (CeO_2 NPs), allowing them to perform multiple antioxidant enzyme functions [13]. Moreover, CeO_2 NPs have shown significant potential in many biomedical applications, including tumors, Alzheimer's, and bowel diseases [14-16]. Antibiotics serve as crucial tools in combating bacterial infections, but their inappropriate usage has resulted in the emergence of numerous multidrug-resistant (MDR) bacteria [17]. Photothermal therapy (PTT) has attracted widespread attention, since it can convert the energy of near-infrared rays (NIR) into physical heat *via* photothermal agents (PTAs), killing bacteria with several advantages including minimal invasiveness, high selectivity, and less potential to induce MDR bacteria [18,19]. As an n-type semiconductor with intrinsic NIR absorption, CuS has been widely used in PTT for cancer and bacterial infections [20,21]. In addition, CuS can release copper ions under NIR irradiation, facilitating cell migration, angiogenesis, and collagen deposition to accelerate wound healing [22], making the precise synthesis of CuS NPs and its nanocomposites (NCs) a research hotspot.

Tannin (TA) is a type of natural, widespread, and biodegradable polyphenolic compound with good antioxidative activities and antibacterial properties [23,24]. TA can be effectively coated on various material interfaces and coordinated with many metal ions, making it a potential linker to prepare multifunctional NCs [25,26]. In this study, mesoporous CeO_2 NPs were simply prepared with

* Corresponding authors.
E-mail addresses: fflgy@126.com (G. Li), jinlin_1982@126.com (L. Jin), shenjl@wiucas.ac.cn (J. Shen).

https://doi.org/10.1016/j.cclet.2024.110286
1001-8417/

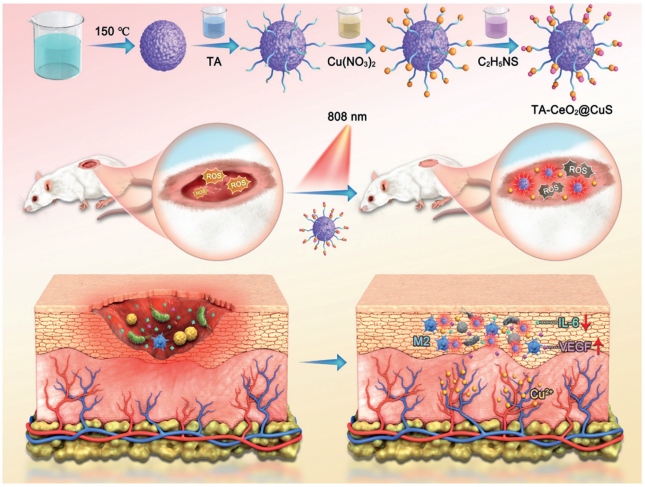

Scheme 1. Schematic illustrations of TA-mediated CeO_2@CuS NC for multimodal synergetic wound therapy.

uniform size and large surface area, and TA was used as a reductant to increase the content of Ce^{3+}. Then, CuS nanocrystals were successfully formed *in situ* on the surfaces of the TA-CeO_2 NPs. As a result, the synthesized TA-CeO_2@CuS NCs exhibited outstanding multimodal wound therapy ability by promoting the synergetic effects of antibacterial, anti-inflammation, and angiogenesis (Scheme 1).

Monodispersed TA-CeO_2@CuS NCs were synthesized in this work by a facile *in situ* method, with the details presented in Supporting information. As shown in Figs. 1a and b, the TA-CeO_2@CuS NCs had a uniform size of ~180 nm and were composed of small crystalline grains about 4 nm, leading to a large Brunner-Emmet-Teller (BET) surface area of 143 m^2/g (Fig. 1c). To demonstrate that TA was modified on the surface and underwent a redox reaction with CeO_2, Fourier transform infrared (FTIR) spectroscopy and absorption spectroscopy were carried out, as shown in Figs. 1e and f. TA-CeO_2 had a wide absorption at the visible light region with a reddish-brown color, as white CeO_2 only absorbed ultraviolet light (Fig. S1 in Supporting information). Meanwhile, many additional peaks were found that belonged to TA in the FTIR spectra of TA-CeO_2. For example, the peaks at 1712 cm^{-1} (C=O), 1196 cm^{-1} (C–O), 1536 and 1614 cm^{-1} (C=C benzene) [27,28]. According to the powder X-ray diffraction (XRD) pattern in Fig. 1d, the characteristic peaks of CeO_2 were clearly assigned to cubic phase (PDF #34-0394). The diffraction peaks of CuS (PDF #01–1281, Fig. S2 in Supporting information) could not be clearly distinguished, likely due to their weak intensity and similar positions with CeO_2. However, the TA-CeO_2@CuS NCs had a smaller surface area than TA-CeO_2 (210 m^2/g) and apparent absorption in the NIR region (Fig. 1e). The distinguished lattice fringes of 0.31 and 0.19 nm could be assigned to the {111} plane of CeO_2 and the {110} plane of CuS, respectively (inset in Fig. 1b). Moreover, the elemental mapping images obtained by high-resolution transmission electron microscope (HTEM) in Fig. 1g directly confirmed the even distribution of Cu and S. All these results indicated that the TA-CeO_2@CuS NCs were successfully prepared.

X-ray photoelectron spectroscopy (XPS) was used to analyze the chemical states of the TA-CeO_2@CuS NCs (Fig. S3 in Supporting information). The v_0, v′, u_0, and u′ peaks corresponding to the binding energies of Ce^{3+}, and the v, v″, v‴, u, u″, and u‴ peaks were attributed to the binding energies of Ce^{4+}(Fig. S3a). The ratio of Ce^{3+} was semi-quantitatively calculated by analyzing the integrated peak area of Ce 3d [29], the ratio of Ce^{3+} in TA-CeO_2@CuS was 45.3%, which was higher than the 41.5% value of CeO_2. As shown in Fig. S3b, two peaks were observed at around 529.6 and 531.5 eV, which were attributed to the lattice oxygen and O–H of surface organic ligand, respectively, and the strong peak at 533.2 eV was attributed to the high binding energy peak from the surface oxygen-deficient species [30]. The results for Cu 2p are shown in Fig. S3c, with peaks at 933.9 and 953.8 eV, and the satellite peak at 945.4 eV was attributed to Cu(II), while the small peaks at 932.7 and 952.6 eV were attributed to Cu(I) [31]. Fig. S3d presents the S 2p spectrum with peaks located at 163.0 and 161.8 eV attributed to the S $2p_{3/2}$ of S^{2-}, and the peak at 168.8 eV could be assigned to the $2p_{1/2}$ of S^{2-} [32]. These results demonstrated the success-

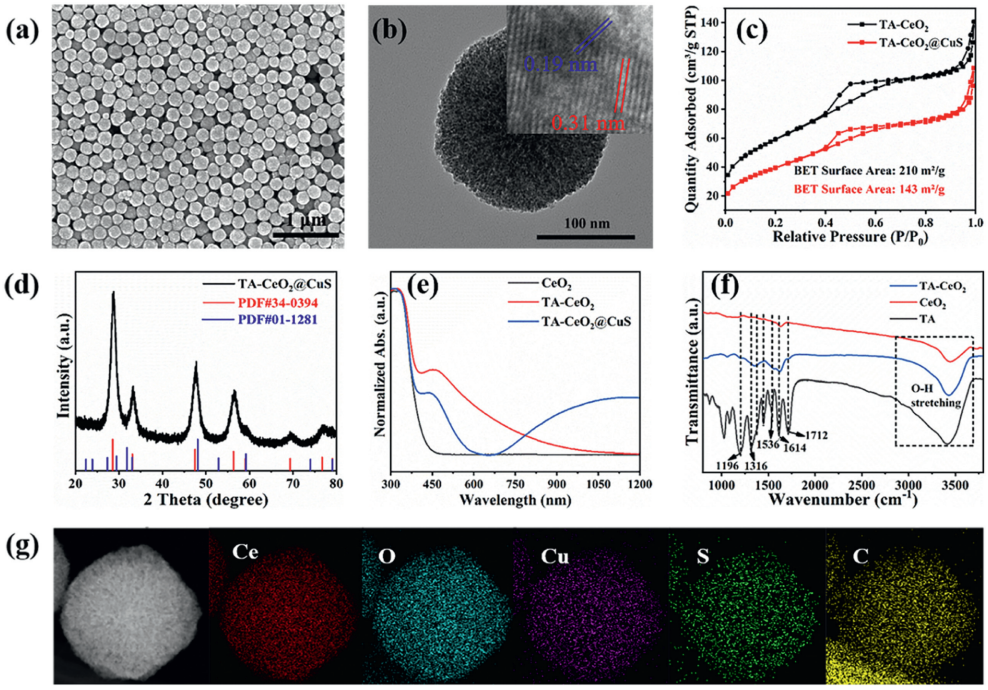

Fig. 1. SEM image (a), TEM image (b), nitrogen adsorption–desorption isotherm (c), XRD pattern (d), normalized absorption spectrum (e), FTIR spectrum (f), and elemental mapping image obtained by HTEM (g).

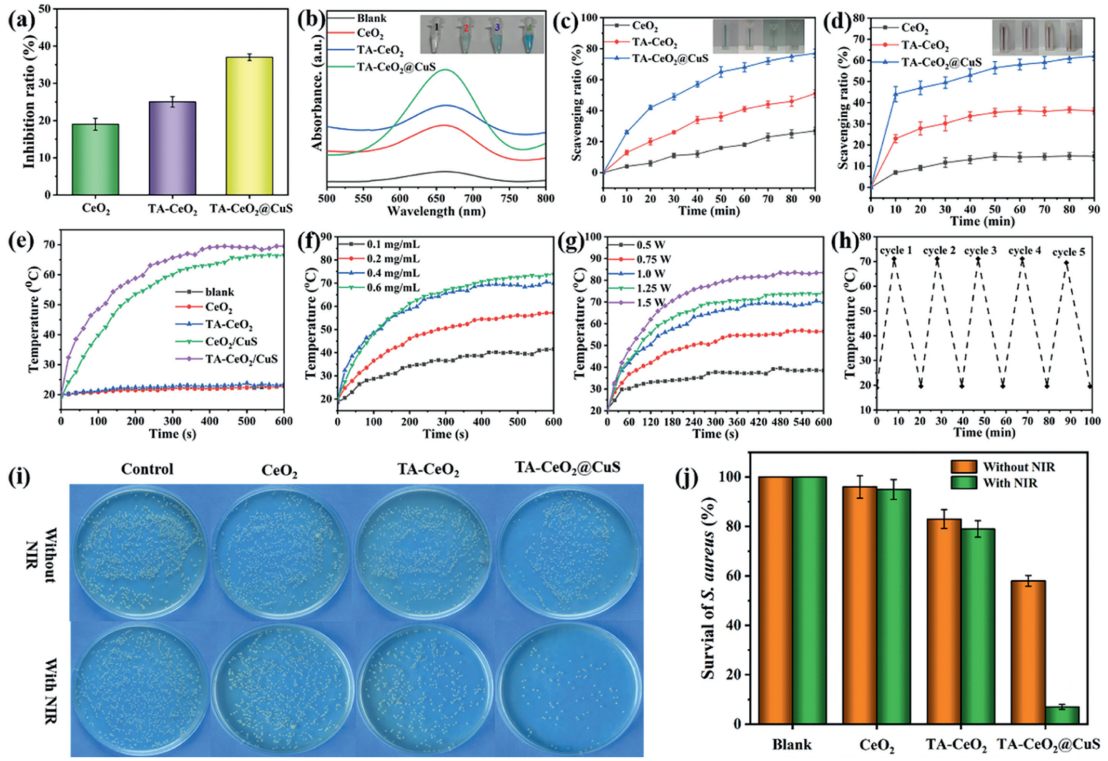

Fig. 2. Nano-enzyme activity tests of SOD (a) and POD (b), the nitrogen radical scavenging tests of $ABTS^{+\bullet}$ (c) and $DPPH^{\bullet}$ (d), evaluation results of the photothermal performance (e–h), representative plate images and statistical analysis of *S. aureus* (i, j). All data are presented as mean ± standard deviation (SD) ($n = 3$).

ful formation of CuS on the CeO_2 surface and the high content of Ce^{3+} and oxygen vacancies in CeO_2 formed through TA reduction. Moreover, the atom ratio of Cu:S was about 1.3:1.0 according to the quantitative XPS results, indicating that redundant copper ions were stored in the TA-CeO_2@CuS NCs.

Excessive ROS in wounds can trigger an inflammatory response, causing cell damage and inhibiting tissue regeneration through increased oxidative stress and lipid peroxidation [33]. The superoxide dismutase (SOD)-like enzyme is a critical scavenger of ROS that can convert superoxide into oxygen and H_2O_2, with activity typically evaluated by an SOD assay kit. Notably, SOD-like enzymes can scavenge $\cdot O^{2-}$ radicals to inhibit the production of blue formazan, with a higher inhibition ratio indicating better SOD-like activity. As shown in Fig. 2a, the TA-CeO_2@CuS NCs demonstrated the highest inhibition ratio, which verified they had excellent SOD-like activity. Similarly, the peroxidase (POD)-like enzyme could convert H_2O_2 to H_2O and O_2, and their activity could be measured by a colorimetric assay method, as the reaction of H_2O_2 with nano-enzyme could convert colorless tetramethylbenzidine (TMB) to blue oxidized TMB (TMBox) with a change in absorbance at 652 nm. As shown in Fig. 2b, the TMB-H_2O_2 solution with TA-CeO_2@CuS presented maximum absorbance and the deepest color, indicating that it had the best POD-like activity.

As two typical nitrogen free radicals, 1,1-diphenyl-2-picrylhydrazyl (DPPH) and 2,2′-azino-bis(3-ethylbenzothiazoline-6-sulfonic acid) diammonium salt (ABTS) were used as model molecules to further evaluate the scavenging capacity of the TA-CeO_2@CuS NCs, and their reaction mechanisms are shown in Fig. S4 (Supporting information). The methanol solution of $DPPH^{\bullet}$ appeared purple with a characteristic absorption peak at 517 nm, while ABTS could be oxidized into $ABTS^{+\bullet}$, and appeared as navy blue with a characteristic absorption peak at 734 nm. After the reaction between $DPPH^{\bullet}$, $ABTS^{+\bullet}$, and the radical scavengers, decreased absorption peaks and significant decolorization were observed. The scavenging ratios at different times are shown in Figs. 2c and d. The TA-CeO_2@CuS NCs exhibited the best scavenging ability of $ABTS^{+\bullet}$, and its scavenging rate was approximately 84% after 100 min, while TA-CeO_2 and CeO_2 were 53% and 26%, respectively. Likewise, the $DPPH^{\bullet}$ test showed similar results, with the TA-CeO_2@CuS NCs demonstrating the highest scavenging ratio and lightest color. Therefore, TA-CeO_2@CuS NCs have excellent free radicals scavenging ability derived from the presence of Ce^{3+}, Cu^{+}, and TA.

According to previous reports, 808 nm NIR with a longer wavelength has shown better tissue penetration and less tissue damage than ultraviolet–visible light, making it more suitable for applications in biological fields [34]. The effects of different factors on the photothermal properties were given in Figs. 2e–g, and the results confirmed the synthesized TA-CeO_2@CuS NCs had excellent photothermal performance with low concentration (≤0.4 mg/mL) and laser power density (≤1 W/cm^2). Moreover, the TA-CeO_2@CuS NCs exhibit outstanding stability, as five heating/cooling cycles were conducted (Fig. 2h). Notably, the TA-CeO_2@CuS solution after NIR irradiation was concentrated at 12,000 rpm twice, and copper ions also were detected by the inductively coupled plasma atomic emission spectra (ICP-AES) in the supernatant, the results indicated that small amounts of copper ions could be released during the laser irradiation process. When the concentration of TA-CeO_2@CuS NCs was 0.2 mg/mL with power density of 1 W/cm^2, the temperature of rats' wound site could be raised to around 50 °C (Fig S5 in Supporting information), which is a suitable temperature for photothermal wound therapy [35].

Antibacterial treatment is a necessary measure in the wound healing process. In this work, we used co-culturing and the plate counting method to explore the antibacterial properties of CeO_2, TA-CeO_2, and TA-CeO_2@CuS. *Staphylococcus aureus* (*S. aureus*) were selected as representative bacteria, and the experiment was divided into two groups without and with NIR irradiation. As shown in Figs. 2i and j, TA-CeO_2@CuS demonstrated the better antibacterial properties than TA-CeO_2 and CeO_2 without 808 nm NIR, due to

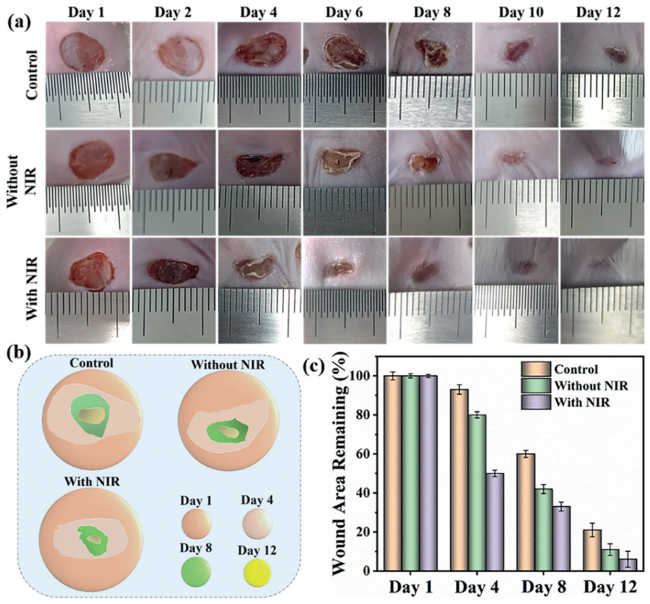

Fig. 3. Representative images of the wound healing process in rats: control, treated with TA-CeO_2@CuS NCs without 808 nm NIR, and treated with TA-CeO_2@CuS NCs with 808 nm NIR (a); diagram of wound changes at different times (b); statistical chart of the residual wound area (c). Data are presented as mean ± SD ($n = 3$).

the effects of TA and copper ions [36,37]. Moreover, TA-CeO_2@CuS also presented better antibacterial activity with the 808 nm NIR, which had high bacterial inhibition rates about 92% for *S. aureus*, due to its outstanding

sistent with the live/dead staining assay and protein leakage assay, and the scanning electron microscope (SEM) was used to study the morphological changes of *S. aureus* (Figs. S6 and S7 in Supporting information). It can be seen that the surfaces of *S. aureus* in the control groups were smooth and had intact structures of bacteria, the collapsed and broken bacteria (red arrow) were observed in the "with NIR" group. Moreover, TA-CeO_2@CuS NC presented high bacterial inhibition rates about 95% for Gram-negative *Escherichia coli* (*E. coli*) (Fig. S8 in Supporting information), which demonstrate it could be used as a new type of antibacterial agent for wound therapy.

To confirm the application value of TA-CeO_2@CuS NCs *in vivo*, skin wound models of rats were established, and *S. aureus* was added to the surrounding wounds. The animal experiments were approved by the Ethics Committee of Zhoukou Central Hospital (No. 2023–001). After successful modeling, the rats were randomly divided into three groups to investigate the effects of TA-CeO_2@CuS NCs on wound healing with and without 808 nm NIR. In the early stage of wound healing (on days 2 and 4), both groups with and without NIR exhibited better healing rates by the antioxidative and antibacterial properties of the TA-CeO_2@CuS NCs (Fig. 3a). To further verify the antibacterial activity *in vivo*, bacteria obtained from the wounds at different times were cultured on agarose medium, and the results showed that the TA-CeO_2@CuS NCs had good antibacterial properties, especially with NIR (Fig. S9 in Supporting information). On day 12, the wound surfaces treated with TA-CeO_2@CuS and NIR were completely healed, demonstrating the best wound healing rates, while the wounds in the other groups were not completely healed. For quantitative analysis, a diagram was obtained of the wound changes at different times and per-

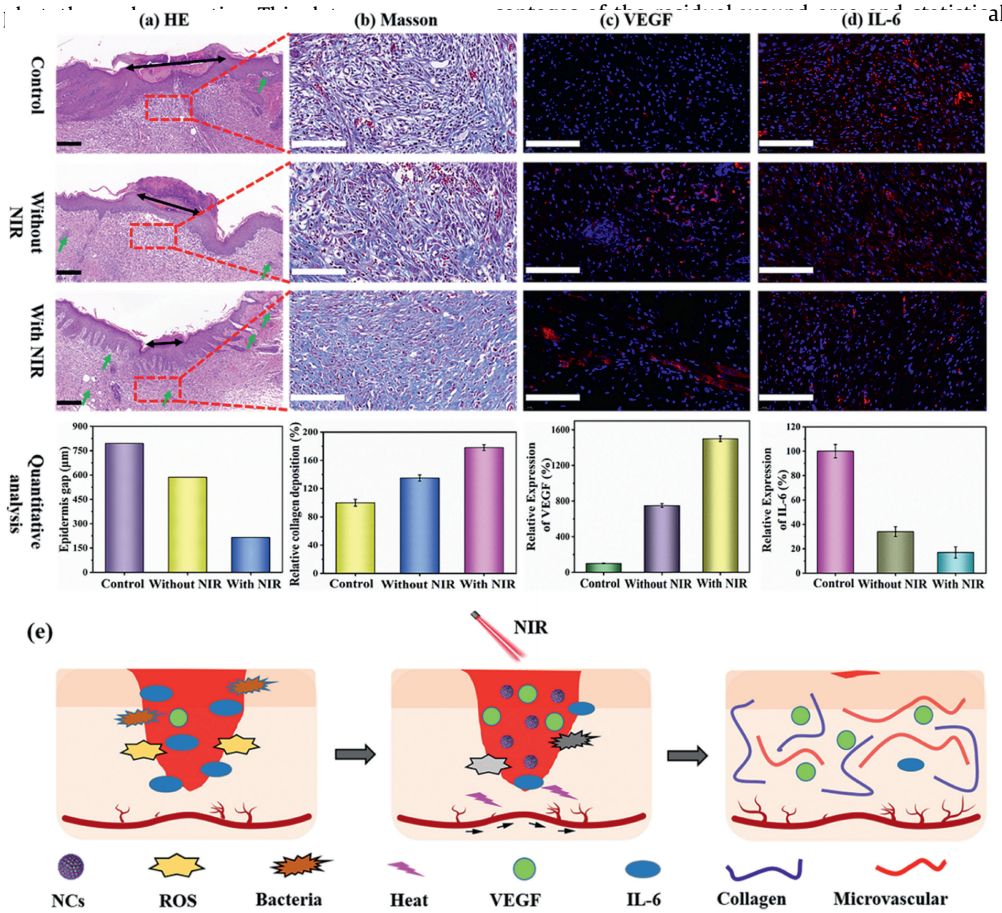

Fig. 4. Histological changes in healed skin tissues and quantitative analysis of the stained images: H&E staining (a), Masson's trichrome staining (b), VEGF staining (c), and IL-6 staining (d) (black scale bar = 200 μm, white scale bar = 100 μm), and mechanism diagram of the TA-CeO_2@CuS NCs promoting wound healing (e). Data are presented as mean ± SD ($n = 3$).

ImageJ software, as shown in Figs. 3b and c, which visually confirmed that the TA-CeO_2@CuS NCs could promote wound healing *in vivo*.

To further evaluate wound recovery and reveal the function mechanism of the TA-CeO_2@CuS NCs, histological changes in healed skin tissues after treatment with different formulas (control, without, and with NIR) were obtained, as shown in Fig. 4. In the hematoxylin and eosin (H&E) staining images (Fig. 4a), all groups had a newly formed epidermis, which was more natural and mature in the group with NIR. This epidermis was present in the form of a minor scar (black arrows) about 265 μm in size, while the group without NIR had a size of 580 μm, and the control group was about 800 μm. In addition, some dermal tissue hair follicles were clearly observed in the group with NIR (green arrows), suggesting the better healing efficiency of the TA-CeO_2@CuS NCs with mild heat stimulation [38]. Collagen is an essential component and function of natural skin, and the formation of collagen at wound sites can serve as an important marker for the remodeling of wound regeneration [39]. Massion's trichrome staining images are shown in Fig. 4b, with the blue color representing newly formed collagen fibers. The relative collagen deposition of the group with NIR was 1.8 times greater than the control group, and the group without NIR was about 1.3 times greater. Angiogenesis is another critical index in wound healing. therefore, the immunofluorescence staining of vascular endothelial growth factor (VEGF) was used to illustrate blood vessel generation, as shown in Fig. 4c. The relative VEGF expression of the group with NIR was 1500%, while the group without NIR was about 700%. According to previous study, one possible reasonable explanation was that the released copper ions of the TA-CeO_2@CuS NCs could promote the proliferation of fibroblast cells and vascular endothelial cells [40]. The immunofluorescence staining revealed that the expression of M1 macrophage marker gene interleukin-6 (IL-6) in the wound area was significantly lower in the group with NIR compared with the other groups (Fig. 4d), confirming the excellent anti-inflammatory ability of the TA-CeO_2@CuS NCs treated with NIR irradiation [41]. In conclusion, TA-CeO_2@CuS NCs provides multifunctional synergistic therapeutic effects of rapid antibacterial and anti-inflammatory, promotion of metabolism and angiogenesis, which are conducive to wound healing (Fig. 4e).

In summary, we successfully synthesized a type of monodispersed TA-CeO_2@CuS NC for multimodal wound therapy. TA acted as a reductant and linker, which facilitated the *in situ* formation of oxygen vacancy and CuS nanocrystals on the surfaces of the mesoporous CeO_2 NPs. The synthesized TA-CeO_2@CuS NCs with a large surface area and uniform size demonstrated a remarkable ROS scavenging ability, which was attributed to the polyphenolic structure of TA and the antioxidant enzyme activity of CeO_2. Moreover, the TA-CeO_2@CuS NCs exhibited photothermal properties and copper ion release induced by NIR irradiation, leading to excellent heat stimulation, antibacterial performance, and angiogenesis ability. Benefiting from these advantages, this type of biomaterial could have favorable application potential in the field of wound therapy.

Declaration of competing interest

The authors declare that they have no known competing financial interests or personal relationships that could have appeared to influence the work reported in this paper.

CRediT authorship contribution statement

Hongwei Ding: Writing – original draft, Resources, Methodology, Investigation, Funding acquisition, Data curation, Conceptualization. **Jingjing Yang:** Visualization, Methodology, Investigation, Data curation. **Yongchen Shuai:** Methodology, Investigation. **Di Wei:** Methodology, Investigation. **Xueliang Liu:** Methodology, Data curation. **Guiying Li:** Supervision, Resources. **Lin Jin:** Validation, Supervision, Methodology, Funding acquisition. **Jianliang Shen:** Writing – review & editing, Resources, Conceptualization.

Acknowledgments

This work is supported by Key Scientific and Technological Project of Henan Province (No. 242102231060), Doctoral Scientific Research Foundation of Zhoukou Normal University (No. ZKNUC2021041), the Program of Innovative Research Team (in Science and Technology) in University of Henan Province (No. 23IRTSTHN008).

Supplementary materials

Supplementary material associated with this article can be found, in the online version, at doi:10.1016/j.cclet.2024.110286.

References

[1] R. Dong, B. Guo, Nano Today 41 (2021) 101290.
[2] J. Wang, X. Ge, Y. Xiang, et al., Chin. Chem. Lett. 36 (2025) 109819.
[3] Y. Wang, K. Liu, W. Wei, H. Dai, Adv. Funct. Mater. 34 (2024) 2402531.
[4] Y. Liang, J. He, B. Guo, ACS Nano 15 (2021) 12687–12722.
[5] Y. Xu, L. Ma, Y. Wang, C. Shi, Chin. Chem. Lett. 36 (2025) 109766.
[6] R. Yu, H. Zhang, B. Guo, Nano-Micro Lett. 14 (2022) 1.
[7] S. Khattak, I. Ullah, H. Xie, et al., Coordin. Chem. Rev. 509 (2024) 215790.
[8] Y. Yang, Y. Liang, J. Chen, et al., Bioact. Mater. 8 (2022) 341–354.
[9] X. Qi, X. Ge, X. Chen, et al., Adv. Funct. Mater. 34 (2024) 2400489.
[10] P. Li, Q. Liu, M. Pei, et al., Chin. Chem. Lett. 35 (2024) 109457.
[11] N.I.M. Fadilah, S.J. Phang, N. Kamaruzaman, et al., Antioxidants 12 (2023) 787.
[12] X. Qi, E. Cai, Y. Xiang, et al., Adv. Mater. 35 (2023) 2306632.
[13] Y. Xue, F. Yang, L. Wu, et al., Adv. Healthc. Mater. 13 (2024) 2302858.
[14] K. Ge, Y. Mu, M. Liu, et al., ACS Appl. Mater. Interfaces 14 (2022) 3662–3674.
[15] S. Zhao, Y. Li, Q. Liu, et al., Adv. Funct. Mater. 30 (2020) 2004692.
[16] X. Zhu, Y. Gong, Y. Liu, et al., Biomaterials 242 (2020) 119923.
[17] Q. Zhao, G. Qing, J. Yu, et al., Chin. Chem. Lett. 35 (2024) 108535.
[18] L. He, D. Di, X. Chu, et al., J. Control. Release 363 (2023) 180–200.
[19] K. Yang, S. Zhao, B. Li, et al., Coordin. Chem. Rev. 454 (2022) 214330.
[20] S. Mo, Y. Song, M. Lin, et al., J. Colloid Interf. Sci. 608 (2022) 2896–2906.
[21] F. Gao, L. Zhu, L. Jiang, et al., Adv. Funct. Mater. 34 (2024) 2312182.
[22] P. Jia, Y. Zou, J. jiang, Small 20 (2024) 2307629.
[23] A. Bigham, V. Rahimkhoei, P. Abasian, et al., Chem. Eng. J. 432 (2022) 134146.
[24] S. Kandhasamy, B. Wu, J. Wang, et al., Int. J. Biol. Sci. 271 (2024) 132506.
[25] Z. Guo, W. Xie, J. Lu, et al., J. Mater. Chem. B 9 (2021) 4098–4110.
[26] H. Wang, X. Li, Y. Jiang, et al., Angew. Chem. 134 (2022) e202200465.
[27] S. Yang, J. Ji, M. Luo, et al., Nanoscale 13 (2021) 16349.
[28] R.G. Dare, E.J. Kolanthai, C.J. Neal, et al., Antioxidants 12 (2023) 190.
[29] X. Liu, X. Wang, C. Qi, et al., Appl. Surf. Sci. 479 (2019) 532–539.
[30] Y. Ru, Y. Chen, X. Yu, et al., Chem. Eng. J. 475 (2023) 146158.
[31] H. Ding, X. Liu, J. Yang, et al., J. Lumin. 263 (2023) 120138.
[32] Y. Xiao, Y. Huang, H. Cheng, et al., Chem. Eng. J. 453 (2023) 139773.
[33] Q. Wang, C. Cheng, S. Zhao, et al., Angew. Chem. 137 (2022) e202201101.
[34] J. Huo, Q. Jia, H. Huang, et al., Chem. Soc. Rev. 50 (2021) 8762.
[35] P. Gao, H. Wang, Y. Cheng, Chin. Chem. Lett. 33 (2022) 575–586.
[36] G. Sathishkumar, K. Gopinath, K. Zhang, et al., J. Mater. Chem. B 10 (2022) 2296–2315.
[37] C. Dong, W. Feng, W. Xu, et al., Adv. Sci. 7 (2020) 2001549.
[38] K. Huang, W. Liu, W. Wei, et al., ACS Nano 16 (2022) 19491–19508.
[39] S. Cheng, L. Chen, F. Gong, et al., Adv. Funct. Mater. 33 (2023) 2212489.
[40] Y. Zhang, C. Xue, Y. Zhang, et al., Chin. Chem. Lett. 35 (2024) 109196.
[41] Y. Li, R. Fu, Z. Duan, et al., ACS Nano 16 (2022) 7486–7502.